JOURNAL OF APPLIED ELECTROCHEMISTRY 13 (1983) 489–505

Water desalting by means of electrochemical parametric pumping. II. Separation properties of a multistage column

Y. OREN, A. SOFFER

Nuclear Research Centre-Negev, Beer Sheva, POB 9001, Israel, 84190

Received 20 April 1982; revised 20 October 1982

Multistage electrochemical parametric pumping has been successfully carried out for water desalination. Separation was effected by electroadsorption–desorption cycles of the ions into and from the electrical double layer of high surface carbon electrodes. At steady state and total reflux, the concentration ratio between the upper and lower heads of the electrochemical column was as high as 150.

Two models for the build up of the concentration profile within the column are presented. The first is based on a solution of the two-phase mass transport equation using the proper boundary and initial conditions. The second treatment is based on the mixed cells assumptions. In both treatments, interphase equilibrium is assumed using the isopotentiograms as the specific equilibrium curves. Use is also made of a fast computer for the simulation of the electrochemical paramatric pumping cycles. The two models are in good agreement with the experimental results particularly in the cases where the initial concentration is high and interphase equilibrium is maintained.

Nomenclature

B_0, B_1	linearization coefficients for the initial concentration distribution
ΔC_f	concentration change in the solution after charge and discharge steps (mol cm^{-3})
C_f, C_s	concentrations at the fluid and solid phases respectively (mol cm^{-3})
C_{fi}, C_{si}	concentrations at the fluid and solid phases respectively in mixed cell i (mol cm^{-3})
C_T, C_B	solution concentrations at the top and bottom heads respectively (mol cm^{-3})
C_K^0	initial concentration of the solution in mixed cell K (mol cm^{-3})
C_e	complete cell electrical capacitance (μF g^{-1})
D	dispersion coefficient (cm^2 s^{-1})
d	length of a single mixed cell (cm)
E_1, E_2	electrical potential of electrode 1 and 2 respectively versus a reference electrode (V)
$\Delta E_1, \Delta E_2$	potential drop across the column during charge and discharge steps respectively (V)
I	charging and discharging current (A)
i	number of mixed cell ($i = 1 \ldots N$)
L	column length
l	dimensionless length coordinate
N	total number of mixed cells
P	Peclet number
Q	solution flow rate (cm^3 s^{-1})
q_e	complete cell charge (C g^{-1})
s	Laplace transform parameter
t, T	dimensional and dimensionless time coordinates respectively
$\Delta R_T, \Delta R_B$	relative concentration charge at the top and bottom respectively
ΔR_{ss}	relative concentration change at steady state
$(\Delta R_{ss})_{lim}$	relative limiting concentration change at steady state

0021–891X/83 $03.00 + .12.

ΔV_F, ΔV_B	volume displaced during forwards and backwards flow steps respectively (cm^3)
V_0	free volume in the column (cm^3)
V_r	the ratio of fluid specific volume V_f to bed specific volume V_s
U	linear axial flow velocity of solution ($cm\,s^{-1}$)
z	dimensional length coordinate
σ	volume displaced during product withdrawal step (cm^3)
ϕ	phase shift between flow and charge or discharge steps
ω	frequency of variations of solution flow and electric current
τ_r	residence time in a mixed cell
τ_D	response time for dispersion process in a mixed cell

1. Introduction

Parametric pumping is a cyclic multistage separation method first introduced by Wilhelm and co-workers in 1966 [1] and studied and extended by many others [2–5]. The method utilizes the capability of changing the distribution coefficient of a species between a fluid and a stationary bed in a column by varying an intensive parameter. The combination of the cyclic variations of the intensive parameter with those of the fluid flow through the column, leads to the buildup of an axial concentration gradient. A variety of intensive parameters were used, namely, pressure [6], concentration [3], temperature [1, 4, 7] and electrical potential [8].

The electrochemical parametric pumping (ECPP) concept was introduced by us in a previous paper [9]. In that work some advantages of the ECPP over other parametric pumping processes were discussed. Water desalting by means of ion electroadsorption on high surface area carbon electrodes was utilized as a test process. The equivalent height of the theoretical plate was formulated and the influence of the electrical resistance–capacitance characteristics of the porous electrodes on the electrical charging–discharging cycles of the ECPP column was analysed.

A desalination batch unit cell that comprises two high surface carbon electrodes is the basic component of the multistage ECPP. The integral adsorptive characteristics of this cell are solely determined by the properties of each one of the two electrodes. In the preceeding paper [10] this dependence has been formulated; efficiency terms for the desalination process have been derived there and their dependence on the working potential range and solution concentration was discussed.

In the present article, the buildup of a concentration gradient along the multistage separation electrochemical parametric pump is studied. Particularly considered is the dependence of the concentration profile on the number of cycles, on the initial concentration, volume of solution displaced during a pumping step and mode of coupling between the electrochemical and pumping steps. Theoretical models of the dynamics of concentration gradient buildup are derived and discussed in the light of experimental results.

2. Experimental procedure

The experimental setup was described in detail in a previous paper [9]. Essentially, two identical high specific surface area carbon electrodes and a porous separator were assembled into a elongated configuration (2 x 10 x 900 mm) to compose a multistage column. The solution flow system is depicted schematically in Fig. 1. The column was operated as an electrochemical parametric pump by means of a microprocessor control system which enabled it to perform the following four operations periodically:

1. Charging (C) by a constant current, i.e., increasing $\Delta E = |E_2 - E_1|$, the potential difference beween the two electrodes to a prescribed value ΔE_1; E_1 and E_2 are the potentials of the two electrodes.
2. Discharging (D) by a constant current to a lower prescribed potential difference, ΔE_2.
3. Pumping the solution forwards (F) through the column by a volume ΔV_F.
4. Pumping the solution backwards (B) through the column by a volume ΔV_B.

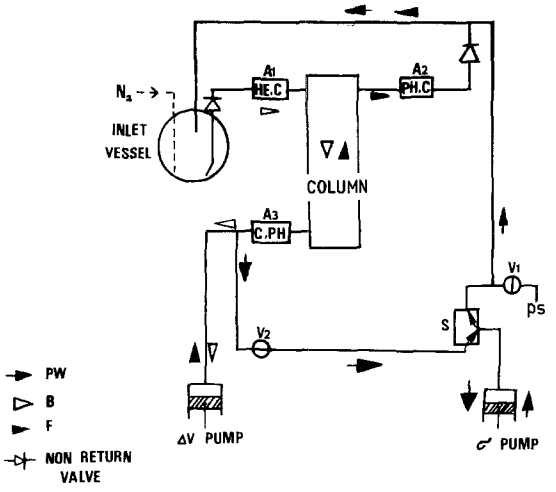

Fig. 1. Flow diagram of the parametric pump. PS, product sampling, PW, product pumping; A, auxilliary compartments containing conductivity cells (C); pH electrode (PH) or heat exchanger (HE); S, three way solenoid valve coupled to product pump (σ); F, direction of pumping forward; B, direction of pumping backwards.

The sequence of the four operations could be selected as desired. Overlapping and consecutive sequences of the electrical and pumping steps were possible. Total reflux operation was ensured by making $\Delta V_F = \Delta V_B$.

Solution concentrations at the bottom and top heads were monitored continuously by an autoranging conductometer. Solutions of NaCl at the initial concentration range of 0.01 to 0.2 mol dm^{-3} were used.

Three total reflux parametric pumping modes were applied:

Mode I. The top head contained a very large volume of solution, thus the concentration could be considered practically constant. The ECPP cycles ran in the sequence C, F, D, B. This resulted as mentioned previously [9] in an increasing concentration at the bottom head.

Mode II. The top and bottom heads had finite volumes and the ECPP step sequence during a cycle was the same as in mode I. Concentration changes were measured at the top and bottom of the column. This mode was the most studied in this work.

Mode III. Complete overlapping of the steps C and F and the steps D and B and a very large solution volume at the top head was attained.

The first mode simulates a feed input at the top head. The second mode is most suitable for obtaining an ultimate concentration difference along the column and the third mode is common to most studies in parametric pumping [2].

Another set of experiments was carried on in order to test the effect of product withdrawal on the concentration gradient. Here, mode I was initially applied with a step sequence C, B, D, F resulting in a concentration decrease in the bottom. After reaching a steady state, the σ pump (Fig. 1) was actuated simultaneously with the B operation of the ΔV pump to withdraw a preset volume at each cycle. The product was sampled from the bottom head where conductivity variations were monitored, and cycled back to the upper head. The σ pump also served to flush the column at the end of each multicycle experiment where a concentration gradient was established. Flushing equalized the concentration throughout the column thus preparing it for the next experiment.

In all the experiments, the constant charging and discharging current density, I, was 0.6 mA cm^{-2} (calculated for the geometrical area) and the potential differences ΔE_1 and ΔE_2 were respectively 1400 and 200 mV. The pumping rate was 1 $cm^3 min^{-1}$ at both forwards and backwards directions.

3. Results and discussion

3.1. *Approaches to the analysis of the buildup of the concentration gradient at the ECPP*

For a first study of the dynamics of the ECPP, we made the following assumptions:

1. The operational steps are sufficiently slow so that local (tranversal) equilibrium is attained. The equilibrium assumption is greatly advantageous since it enables the use of the isopotentiograms (adsorption isotherm at constant ΔE), which can be obtained from separate batch process experiments [10], as working curves for the ECPP steps.

2. The mixing of the solution at the heads is completed prior to each pumping step.

3. Molecular diffusion is sufficiently small so practically no axial mixing occurs when there is no flow of solution. The column is thin and long enough to render this assumption acceptable.

4. The ratio U/D (U, axial velcoity; D, dispersion coefficient) is constant. Nevertheless, precautions have been taken to keep the flow rate Q constant during the pumping steps so that any eventual dependence of U/D on Q will not affect the experimental results.

In the present work, two commonly used theoretical models of fixed bed columns are adopted after modifying the basic flow equations in compliance with the ECPP requirements. The first one is the continuum model according to which the mass balance equation for an absorbing bed:

$$U\frac{\partial C_f}{\partial z}+\frac{\partial C_f}{\partial t}+V_r\frac{\partial C_s}{\partial t}-D\frac{\partial^2 C_f}{\partial z^2}=0 \tag{1}$$

has to be solved for the specified initial and boundary conditions. Here C_f is the solution concentration, C_s the adsorbate concentration on the fixed bed and V_r the ratio of bed to fluid specific volumes, V_s/V_f.

The other model, first proposed by Kramers and Alberda [11], is based on the division of the column into N ideally mixed cells of length d, between which mass transfer occurs due to flow of solution along the series of cells and to the dispersion process. Several workers adopted this approach and Gupta and Sweed [12] applied it to nonequilibrium processes in parametric pumping.

The solution concentration in cell i, C_{fi} is by definition equal to its exit concentration. Thus, we can write for a nonadsorbing bed,

$$\frac{dC_{fi}}{dt}=(C_{f(i-1)}-C_{fi})/\tau_r \tag{2}$$

where $C_{f(i-1)}$ is the concentration of the entering solution. The internal residence time τ_r should be:

$$\tau_r=\frac{d}{U}=\frac{V_0}{NQ} \tag{3}$$

where V_0 is the total free volume of the solution in the column. For the present case of adsorbing bed the mass conservation law, Equation 2, is replaced by:

$$\frac{dC_{fi}}{dt}=\frac{C_{f(i-1)}-C_{fi}}{\tau_r}-V_r\frac{dC_{si}}{dt} \tag{4}$$

where C_{si} is the adsorbate concentration in the fixed bed in cell i.

According to Klinkenberg and Sjenitzer [13], the time τ_r should be equal to the response time of the dispersion process of the system:

$$\tau_D=\frac{d^2}{2D}.$$

Using Equation 3, the cell length is obtained:

$$d=\frac{2D}{U} \tag{5}$$

Thus, a column of length L will contain N ideally mixed cells expressed by

$$N=\frac{L}{d}=\frac{LU}{2D}. \tag{6}$$

An expression which relates the time derivation of C_s in Equations 1 and 4, with C_f has to be derived now. This is done as follows: The adsorbate concentration C_s is related to the solution concentration by means of the isopotentiograms [10] namely:

$$C_s = F(C_f, \Delta E). \tag{7}$$

The use of this equilibrium expression in a system which is intrinsically dynamic is justified since the pumping steps were taken long enough (about 5 min) to enable equilibration of the system prior to the subsequent charging or discharging steps. It is easily estimated that at electrolyte concentrations above 0.1 mol dm^{-3} the amount of electrolyte in the pores which is immediately available for adsorption is considerably larger than the amount adsorbed or desorbed during the charge or discharge steps. Upon such conditions the equilibration time should be comparable to the R–C characteristic time of the double layer capacitance and solution resistivity. This time is experimentally measurable and was about 30 s, considerably smaller than the above mentioned pumping time.

The time derivative of Equation 7 gives:

$$\left(\frac{\partial C_s}{\partial t}\right)_z = \left(\frac{\partial C_s}{\partial C_f}\right)_{\Delta E}\left(\frac{\partial C_f}{\partial t}\right)_z + \left(\frac{\partial C_s}{\partial \Delta E}\right)_{C_f}\left(\frac{\partial \Delta E}{\partial t}\right)_z. \tag{8}$$

The derivative $(\partial C_s/\partial C_f)_{\Delta E}$ is the slope of the isopotentiogram (Fig. 11 in reference [10]) and $(\partial C_s/\partial \Delta E)_{C_f}$ is the slope of the experimental curves of the amount adsorbed against potential (Fig.5 in reference [10]). The derivative $(\partial \Delta E/\partial t)_z$ may have the form $I\,(\partial \Delta E/\partial q_e)_z$, where q_e is the complete cell charge [10], I is the electrical current and $(\partial \Delta E/\partial q_e)_z$, by definition, is the reciprocal of the complete cell electrical capacitance, C_e, which was shown to be constant over a wide range of ΔE [10].

Equation 8 will consequently be written as follows:

$$\left(\frac{\partial C_s}{\partial t}\right)_z = \left(\frac{\partial C_s}{\partial C_f}\right)_{\Delta E}\left(\frac{\partial C_f}{\partial t}\right)_z + \left(\frac{\partial C_s}{\partial \Delta E}\right)_{C_f}\frac{I}{C_e} \tag{9}$$

Upon substitution of Equation 9 in Equation 1, one obtains,

$$U(\omega t + \phi)\frac{\partial C_f}{\partial z} - D\frac{\partial^2 C_f}{\partial z^2} + (S+1)\frac{\partial C_f}{\partial t} + V_r\left(\frac{\partial C_s}{\partial \Delta E}\right)_{C_f}\frac{I(\omega t)}{C_e} = 0 \tag{10}$$

where

$$S = V_r\left(\frac{\partial C_s}{\partial C_f}\right)_{\Delta E} \tag{11}$$

In Equation 10 we put $U = U(\omega t + \phi)$ and $I = I(\omega t)$ which are general periodic functions of the solution linear flow velocity and of the electric current respectively, with a frequency ω and a phase shift ϕ. Thus Equation 10 is a general mass balance expression, valid for any combination of the four ECPP steps. If explicit periodic expressions for U and I are substituted in Equation 10, a solution for the concentration distribution along the column as a function of the number of cycles may be obtained. Since Equation 10 is a non-linear periodic differential equation, it is very difficult to solve it by simple and common methods. Similar difficulties may arise upon applying the same considerations to Equation 4.

A simpler procedure for the analysis of the ECPP may be proposed for the case where the ECPP steps do not overlap. In this case, each step may be analysed separately for the concentration distribution along the column. The concentration distribution obtained at the end of a step, provides the initial conditions for the next step. Since during the solution flow steps (F and B), $I = 0$ and U is no longer periodic, Equation 10 reduces to:

$$U\frac{\partial C_f}{\partial z} - D\frac{\partial^2 C_f}{\partial z^2} + (1+S)\frac{\partial C_f}{\partial t} = 0 \tag{12}$$

and Equation 4 reduces to:

$$\tau_r(1+S)\frac{dC_{fi}}{dt} = C_{f(i-1)} - C_{fi}. \tag{13}$$

These equations when provided with the appropriate initial and boundary conditions may be solved for the concentration distribution along the column during steps F and B. During the charging (C) and discharging (D) steps there is no flow of solution through the column. As was shown previously [10] the slopes of the isopotentiograms do not change over a wide range of concentration. It follows therefore that during steps C and D, there is respectively a decrease and an increase of the solution concentration by the same extent along the column.

Since there are many cycles in each ECPP run, the computations of the concentration distribution at the end of each step in the successive cycles has to be done by a fast computer.

In the following sections the solution of Equations 12 and 13 for the F and B steps will be given and the model simulation procedure will be outlined.

3.2. *The continuum model of the flow steps*

The substitution of the dimensionless magnitudes:

$$T = t/\tau; \quad l = z/L; \quad \delta = L/U\tau \tag{14}$$

and

$$P = UL/4D \tag{15}$$

in Equation 12 gives:

$$\frac{1}{4P}\frac{\partial^2 C_f}{\partial l^2} - \frac{\partial C_f}{\partial l} = \alpha\frac{\partial C_f}{\partial T} \tag{16}$$

where P is the Peclet number, τ is the flow time of the displacement volume ΔV, L is the column length and

$$\alpha = \frac{(1+S)L}{\tau U} = \frac{1+S}{\delta} \tag{17}$$

The backwards pumping will be considered positive (i.e., pumping from $l = 0$ to $l = 1$). The boundary condition for backwards pumping results from the constant concentration C_T at the top ($l = 0$) of the column. The mass balance equation at $l = 0$ then read:

$$UC_f - D\frac{\partial C_f}{\partial z} = UC_T, \tag{18}$$

and in terms of Equations 14 and 16:

$$C_f - C_T = \frac{1}{4P}\frac{\partial C_f}{\partial l} \tag{19}$$

For $l = 1$ we adopted, after Brenner [14] the boundary condition:

$$\frac{\partial C_f}{\partial l} = 0; \tag{20}$$

since the choice of a condition similar to that of Equation 18, which is also physically sound, would lead to concentration profiles involving extrema [15]. For a forward pumping, C_T should be replaced by C_B, the constant concentration at the bottom head and the boundary conditions Equations 18 and 20 will be related to the bottom head and the top of the column respectively. Although Brenner considered a column with a nonadsorbing bed, our basic differential equation and boundary conditions proved similar to his, apart from the constant multiplier $1 + S$. The similarity results from the use of linear isopotentiograms to replace C_s by C_f. Our initial conditions are, however, different. We may write:

$$C = C_f - C_T \tag{21}$$

and

$$C = V(l, T) \exp\left(2Pl - \frac{PT}{\alpha}\right). \tag{22}$$

Differentiation of the last equation and its substitution in Equation 16 gives:

$$\frac{1}{4P\alpha} \frac{\partial^2 V}{\partial l^2} = \frac{\partial V}{\partial T}. \tag{23}$$

The initial conditions in terms of the variable V, which is obtained by taking $T = 0$ in Equation 22 is:

$$V(l, 0) = [f(l) - C_T] \exp(-2Pl) \tag{24}$$

where $f(l)$ is any initial concentration distribution function. The boundary conditions given by Equations 19 and 20, will become respectively:

$$\frac{\partial V}{\partial l} - 2PV = 0 \quad \text{for} \quad l = 0 \tag{25}$$

and

$$\frac{\partial V}{\partial l} + 2PV = 0 \quad \text{for} \quad l = 1 \tag{26}$$

The general solution of Equation 23 with the initial and boundary conditions 24–26 is given by Carslaw and Yeager [16] for a case of thermal irradiation of a slab and is suitable for any initial concentration distribution. This fact is of special importance since the initial conditions change from step to step during the parametric pumping process. The crucial drawback of this solution is that it converges extremely slowly for the high Peclet numbers and the normalized time values relevant to this work (a Peclet number in the range of 10–20 was obtained from flow experiments that will be described later). We tried therefore to solve Equation 23 via a Laplace transform by introducing an approximation for high Peclet numbers and assuming a linear initial concentration distribution profile, as outlined in the Appendix. The solution provides the concentration distribution along the column at any time during the flow steps and contains the Peclet number as a single parameter which has to be optimized in the course of comparing the model with the experimental results.

3.3. *Preliminary estimation of Peclet number*

For a zero electric current (open circuit), the ECPP column behaves as an ordinary column with an adsorbing bed. It is possible, therefore to perform a unidirectional flow experiment in order to estimate the Peclet number. This may then be compared to the Peclet number obtained from the best fit of the multi-cycle ECPP model to experimental data. Brenner [14] provided a solution for flow through a column with a nonadsorbing bed initially at constant concentration C_0 and flushed with a solution at a different concentration C_T. The basic mass transport equation in this case is:

$$U\frac{\partial C_f}{\partial z} + \frac{\partial C_f}{\partial t} - D\frac{\partial^2 C_f}{\partial z^2} = 0. \tag{27}$$

Using the linear isopotentiograms obtained by us [10], Equation 12 for the adsorbing bed assumes the form:

$$U\frac{\partial C_f}{\partial z} + (1 + S)\frac{\partial C_f}{\partial t} - D\frac{\partial^2 C_f}{\partial z^2} = 0, \tag{28}$$

which is identical to Equation 27 except for the constant $1 + S$. Furthermore, our measurements revealed that S is only about 0.015 and can therefore be neglected in Equation 28. We may consequently use the results obtained by Brenner (Table 2 in reference [14]) without any change. Figure 2 gives

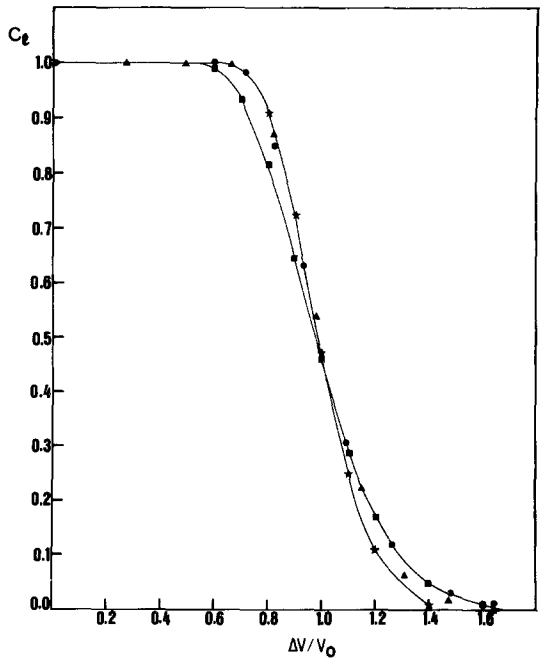

Fig. 2. Dimensionless concentration against relative displacement volume for continuous flow experiments: ★ $P = 10$; ■ $P = 20$, after Brenner [14]; ●, ▲ experimental.

the dimensionless concentration $c_l = (C_l - C_T)/(C_0 - C_T)$ versus the relative solution volume displacement $\Delta V/V_0$ according to Brenner's data for the Peclet numbers 10 and 20 (C_l is the concentration at the outlet of the column). It also gives the results of two identical unidirectional flow experiments in our setup with flow rate of 1 $cm^3 min^{-1}$. It is evident that the Peclet number which corresponds to flow and dispersion conditions in our experiments is within 10–20.

3.4. *The mixed cell model of the flow steps*

This model has been outlined in Section 3.1. There are N-1 equations of the form of Equation 13 which will be written as

$$\frac{dC_i}{d\tau} = C_{i-1} - C_i, \quad i \neq 1 \tag{29}$$

where the suffix f was omitted for simplicity, and one equation of the form,

$$\frac{dC_1}{d\tau} = C_T - C_1, \quad i = 1. \tag{30}$$

The time τ is defined here as

$$\tau = \frac{t}{\tau_r(1+S)} \tag{31}$$

In these equations the cells are numbered in the direction of flow. They are therefore valid for both forward and backward pumping directions.

Equations 29 and 30 are solved by Laplace transformations. Summarizing and reversing the transforms we obtain:

$$C_i = \sum_{K=1}^{i} \frac{\tau^{i-K} C_K^0 e^{-\tau}}{(i-K)!} + C_T \left\{1 - e^{-\tau}\left(1 + \frac{\tau}{1!} + \frac{\tau^2}{2!} + \cdots \frac{\tau^{i-1}}{(i-1)!}\right)\right\} \tag{32}$$

Where C_K^0 is the initial concentration of cell K. Thus, the concentration C_i during the (dimensionless) flow time τ at a location i along the column is given in terms of τ and the initial concentration profile C_K^0 ($K = 1 \ldots i$). The concentration at the end of the flow time $t_F = \Delta V/Q$ is obtained by substituting:

$$\tau = \frac{\Delta VN}{(1+S)V_0} \tag{33}$$

in Equation 32. Equation 33 is obtained by substituting t_F in Equation 31. The number of ideally mixed cells, N, is the only unknown parameter that has to be adjusted in Equation 32 to fit the experimental results.

An interesting and simple relation between N and the Peclet number, P, may be obtained by means of Equations 6 and 15, namely,

$$N = 2P \tag{34}$$

This relation will be utilized later in the comparison of the two models. The mixed cell model, as compared to the continuum model, has the adavantage of mathematical simplicity that avoids the necessity of profile linearization applied to the continuum model.

3.5. *Model simulation procedure*

The simulation procedure performed with a fast computer comprises the following steps:

1. The computer is provided with the basic information for computations, i.e., Peclet number or number of mixed cells (estimated from single flow experiments), slope of isopotentiograms (taken from the experimental results [10] as 0.015), number of cycles, relative displacement volume $\Delta V/V_0$, volume of column heads, initial concentration and concentration change after charge or discharge steps calculated from the isopotentiograms.

2. Simulation of the charge step, i.e., the concentration change in the solution that occurs upon adsorption on the electrodes. This change is given by:

$$^*\Delta C_f = V_r \int_{\Delta E_1}^{\Delta E_2} \frac{dC_s}{d\Delta E}\, d\Delta E \tag{35}$$

and was calculated from the experimental isopotentiograms.

3. Linearization of the profile using only the linear portion (Equation A10) of the polynomial in a least square fitting program in the case of the continuous model.

4. A forwards flow simulation, at the end of which concentration changes are computed by means of the solution of either Equation 16 for the continuum model or Equations 29 and 30 for the mixed cells model.

5. Computation of effluent concentration against time for the forward flow taking the final value at the column edge concentration. Integration of the corresponding curve to calculate the average head concentration change. In the following discussion the experimental and calculated concentrations at the head of the column are presented in terms of dimensionless ratios, i.e., $\Delta R_T = (C_T - C_0)/\Delta C_f$ for the top head and $\Delta R_B = (C_B - C_0)/\Delta C_f$ for the bottom head.

6. Discharge simulation, similar to charge (step 2).

7. Profile linearization and B step simulation similar to steps 3 and 4 above, The sequence 2–7 is then repeated cycle by cycle.

The two models presented may in principle provide the concentration profiles along the column at any moment during ECPP cycling. In practice only the concentrations at the heads at the end of each cycle can be compared with experimental results.

*ΔC_f is equivalent to $C_0 - C_{\Delta E}$ in reference [9], Equation 3.

3.6. *Results of model simulation and their comparison with experimental data*

The theoretical concentration profile buildup for the mixed cell model in the case of a high relative displacement volume is given in Fig. 3. The horizontal section is due to the pumping of solution from the head into the column. The inflection point is located slightly before the point which corresponds to $\Delta V/V_0$ (= 0.5) since the former higher and steeper profile is 'pushed' by the incoming solution. In Fig. 4 similar curves are given but for a rather smaller relative displacement volume and for several cycle numbers. Unlike Fig. 3, the horizontal portion can hardly be observed in Fig. 4 because of the small relative displacement. The following features are noteworthy: (a) The buildup of concentration changes starts close to the column edges as observed from the curves for cycle numbers 10 and 50. (b) The profile behaves symmetrically with respect to the centre of the column (with almost equal head volumes). (c) The profile approaches a linear form after a considerable number of cycles had elapsed. (d) The profile becomes steeper as the cycle number increases until steady state is achieved.

In Fig. 5 are depicted the results of theoretical calculations obtained from the mixed cells and the continuum models for the same conditions and for $N = 2P$. As may be seen, there is a good agreement between the two models. The symmetries of the curves shown in Fig. 5 with respect to $\Delta R = 0$ and of the concentration profiles shown in Fig. 4 with respect to the centre of the column are interpreted as follows: as was discussed in the preceeding paper [10], the isopotentiograms are parallel, namely $(\partial C_s/\partial C_f)_{\Delta E}$ is constant. As a result, the concentration change during the charge process is constant throughout the column. An equal and opposite concentration change occurs during the discharge process. There is therefore a constant difference between the concentration of the solution along the column during the backwards and the forwards flow steps. The constant difference law is expressed as,

$$K_{\mathrm{ECPP}} = C_f^{\mathrm{B}} - C_f^{\mathrm{F}} = \Delta C_f \tag{36}$$

where C_f^{B} and C_f^{F} are the concentrations along the column at any time during the backward and forwards flows respectively and K_{ECPP} is constant.

If the volumes of the heads were equal, the initial concentration gradient buildup at the edges of the column would be the same. Dispersive forces would therefore introduce the profile into the column with symmetry kept throughout since the dispersive force itself is proportional to the concentration gradient. However, the distortion of symmetry as depicted in Figs. 6 and 7 for a symmetric column (equal head volumes), would indicate inadequacy of the assumption of constant $(\partial C_s/\partial C_f)_{\Delta E}$. Moreover, distortion of symmetry is larger at lower initial concentration as can be recognized upon comparing

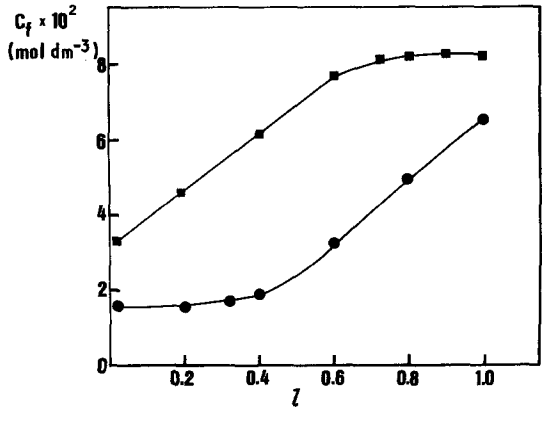

Fig. 3. Theoretical concentration profile as calculated for the mixed cells model in mode II. Initial concentration: $C_0 = 0.05$ mol dm^{-3}; cycle number: 150; number of mixed cells: $N = 25$; $\Delta V/V_0 = 0.5$. •, after charge; ■, after discharge.

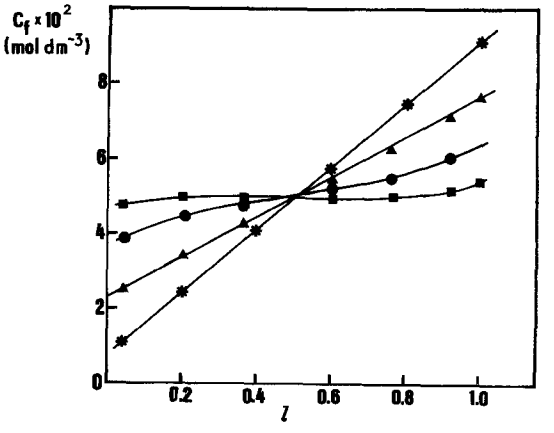

Fig. 4. Theoretical concentration profiles after discharge for different cycle numbers in the mixed cells model in mode II; $\Delta V/V_0 = 0.03$; $C_0 = 0.05$ mol dm^{-3}; $N = 25$; cycle number; ■, 10; •, 50; ▲, 150; ∗, 500.

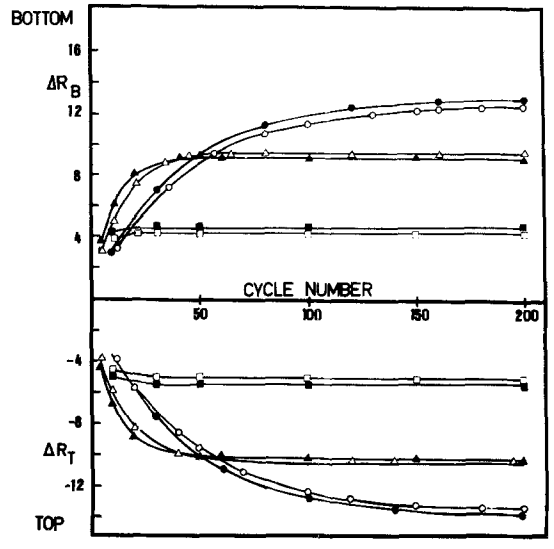

Fig. 5. Relative concentration change at the column heads against cycle number as calculated from the models for mode II. The continuous model ($P = 12.5$) in represented by the symbols ●, ▲ and ■. The mixed cell model ($N = 25$) by the symbols ○, △ and □. ○, ●, $\Delta V/V_0 = 0.125$; △, ▲, $\Delta V/V_0 = 0.5$; □, ■, $\Delta V/V_0 = 1.0$.

these figures. This difference may be explained by the existence of a theoretical limit for the constancy of $(\partial C_s/\partial \Delta E)_{C_f}$ during the charge process, set by the inequality,

$$V_r \int_{\Delta E_1}^{\Delta E_2} \left(\frac{\partial C_s}{\partial \Delta E}\right)_{C_f} d\Delta E \leqslant C_f. \tag{37}$$

This inequality results from the requirement that there should be sufficient material in the solution to be adsorbed during the charge process. In cases of low initial concentration, extreme dilution at the upper head of the column violates inequality Equation 37. Under such conditions, part of the column

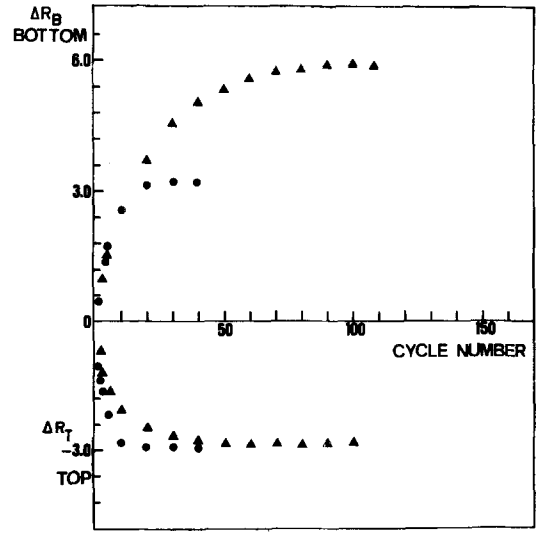

Fig. 6. Relative concentration changes for mode II experiments. $C_0 = 0.01$ mol dm^{-3}; $I = 0.6$ mA cm^{-2}; ●, $\Delta V/V_0 = 0.5$; ▲, $\Delta V/V_0 = 0.125$.

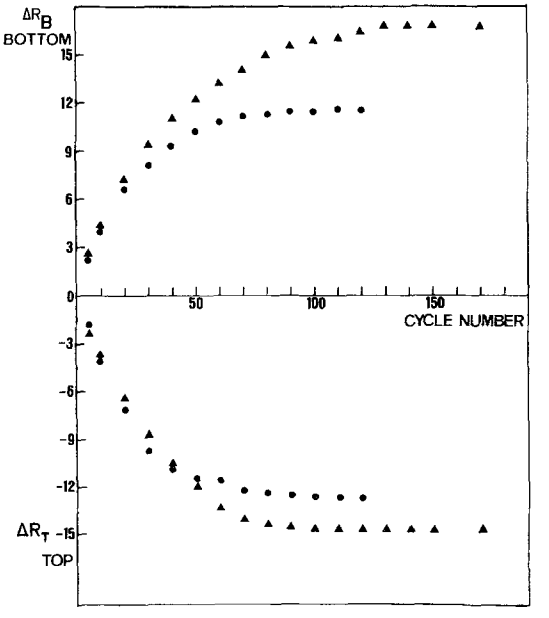

Fig. 7. Relative concentration changes for mode II experiments. $C_0 = 0.05$ mol dm^{-3}; $I = 0.6$ mA cm^{-2}; ●, $\Delta V/V_0 = 0.5$; ▲, $\Delta V/V_0 = 0.25$.

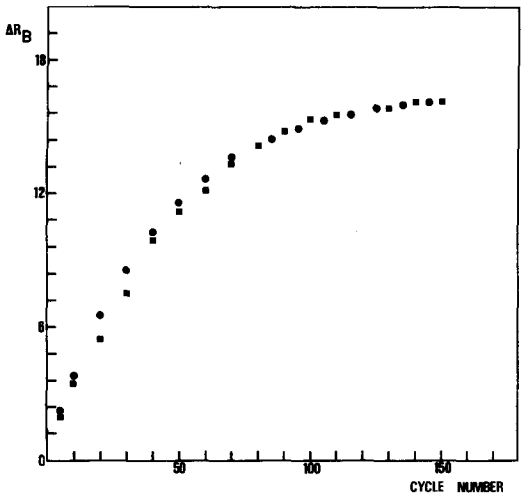

Fig. 8. Comparison of experimental with theoretical results, mode I. $C_0 = 0.2$ mol dm^{-3}; $\Delta V/V_0 = 0.5$; ■, experimental; ●, theoretical results from mixed cell models. $N = 36$.

is practically deactivated since the solution conductivity reaches a very low level and electric charge is preferably delivered to the more conductive parts of the column.

In order to examine the models under conditions far from the limiting concentration law given by Equation 37, we chose mode I experiments with constant concentration maintained at the more diluted edge of the column [18]. The concentration along the column could then only increase in the course of the ECPP process. A comparison of the experimental results with the mixed cell model is given in Fig. 8 for an optimized number of mixed cells, found to be 36. It is clear from this figure that the fit is satisfactory. The correspondence between the mixed cells and the continuum models has already been demonstrated in Fig. 5. It should be recalled that the Peclet number 18 which corresponds to 36 mixed cells falls within the range obtained from the single flow experiment treated according to the continuum model (Fig. 2).

It is noteworthy that the ECPP may be considered as a countercurrent process in which the solution pumped forwards and the backwards play the role of the two fluid phases. While regular countercurrent processes are governed by a distribution constant expressed as a ratio of the concentrations in the two streams [19], the ECPP process may be considered to be governed by the constant difference law expressed in Equation 36.

3.7. *The dependence of the steady state concentration on the relative displacement volume*

The theoretical results presented in Fig. 5 predict higher steady state concentrations and a slower approach to steady state for smaller relative displacement volumes. These features are observed in all experimental results, i.e., Figs. 7, 9 and 10. Exceptions are the experiments in which extreme dilution caused deactivation of part of the column (Fig. 6).

From the trend of ΔR_{ss}, the relative concentration change at steady state, expressed by both theoretical and experimental results, it may be inferred that regardless of the initial concentration, ΔR_{ss} should approach a limiting value as $\Delta V/V_0$ becomes very small. It is possible to derive an explicit expression for this limiting value, $(\Delta R_{ss})_{lim}$ as follows*:

The dispersive and flow fluxes during the forwards step are $-(D/L)(dC_f^F/dl)$ and UC_f^F and during the backwards step, $-(D/L)(dC_f^B/dl)$ and UC_f^B respectively. At steady state the net flux during a cycle should be zero, thus,

* An explicit expression could not however be derived for ΔR_{ss} by the models discussed because the computation of the concentrations as a function of the cycle number is done by a stepwise procedure.

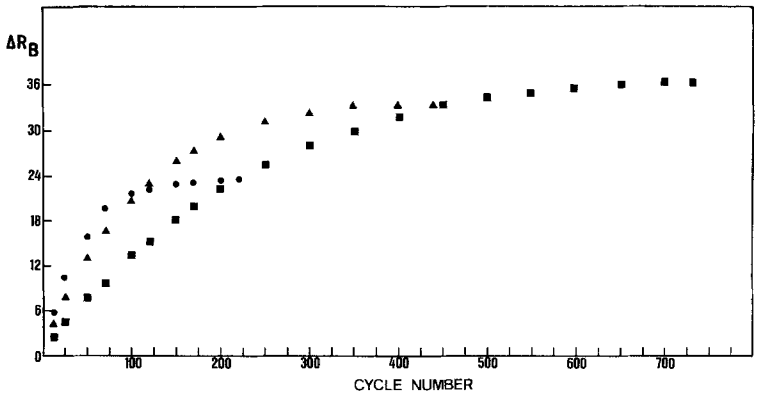

Fig. 9. Relative concentration variations at the bottom of the column, mode I experiment. $C_0 = 0.01$ mol dm^{-3}; $I = 0.6$ mA cm^{-2}; •, $\Delta V/V_0 = 0.5$; ▲, $\Delta V/V_0 = 0.25$; ■, $\Delta V/V_0 = 0.125$.

$$UC_f^B - UC_f^F - \frac{D}{L}\left(\frac{dC_f^F}{dl} + \frac{dC_f^B}{dl}\right) = 0 \tag{38}$$

From the constant difference law (Equation 36) it follows that $C_f^B - C_f^F$ is constant and equal to ΔC_f. Moreover, when $\Delta V/V_0$ is very small the concentration profile at steady state is linear thoughout the column (see Fig. 4 and related discussion) thus,

$$\frac{dC_f^F}{dl} = \frac{dC_f^B}{dl} = \frac{dC_f}{dl} \tag{39}$$

It follows that,

$$\frac{dC_f}{dl} = \frac{UL}{2D}\Delta C_f = N\Delta C_f = 2P\Delta C_f. \tag{40}$$

The last two equalities at the right side of Equation 40 are according to Equations 6 and 15. Integration of Equation 40 along the column yields,

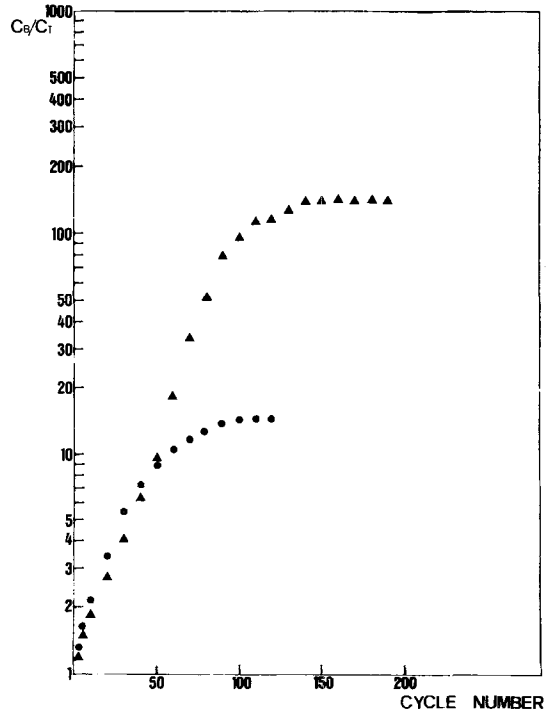

Fig. 10. Variation of concentration ratio with the number of cycles; mode II experiments. $C_0 = 0.05$ mol dm^{-3}; $I = 0.6$ mol cm^{-2}; •, $\Delta V/V_0 = 0.5$; ▲, $\Delta V/V_0 = 0.25$.

Table 1. Relative concentration changes at steady state

Mode	C_0 (mol dm^{-3})	$\Delta V/V_0$	ΔR_{ss}
I	0.01	0.5	23
I	0.05	0.5	22
I	0.2	0.5	17
II	0.05	0.5	25
I	0.01	0.25	33
I	0.05	0.25	32
II	0.05	0.25	31
I[a]	–	$\rightarrow 0$	36

[a] Theoretical limiting value from Equation 41.

$$(\Delta R_{ss})_{lim} = \frac{C_B - C_T}{\Delta C_f} = 2P = N \tag{41}$$

This equation gives a new physical meaning to the Peclet number and the number of mixed cells of the ECPP.

An interesting point is revealed upon examining the experimental ΔR_{ss} values of different $\Delta V/V_0$ and initial concentration values. As may be observed in Table 1, the relative steady state concentration change remains practically constant for a given $\Delta V/V_0$ when the initial concentration is varied. Clearly this results from the relevance of the constant difference law to the desalination power of the ECPP. Also, Table 1 reveals that ΔR_{ss} increases as $\Delta V/V_0$ decreases and approaches the theoretical limiting value calculated by means of Equation 41.

If the ECPP column (which obeys the difference law) is considered to be equivalent to a counter-current column with two opposing streams, ΔC_f becomes the equilibrium concentration difference of a batch unit cell so that N (or $2P$) become the number of the theoretical plates of the column. We cannot, however claim this term is also valid for cases of finite $\Delta V/V_0$. Nevertheless, the relative concentration changes given in Table 1 remain an ultimately important criterion for the separative capability of the column.

3.8. *Some further experimental results*

Figure 11 shows the results of cycling the column according to mode III where complete overlap was maintained between the charging, discharging and pumping steps. The rate of achieving steady state is almost the same as in a similar experiment performed in mode II. However, the limiting relative con-

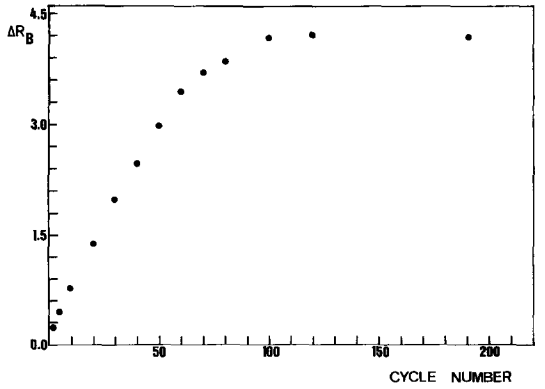

Fig. 11. Relative concentration variations at the bottom of the column; mode III. $C_0 = 0.05$ mol dm^{-3}; $\Delta V/V_0 = 0.5$; $I = 0.6$ mA cm^{-2}.

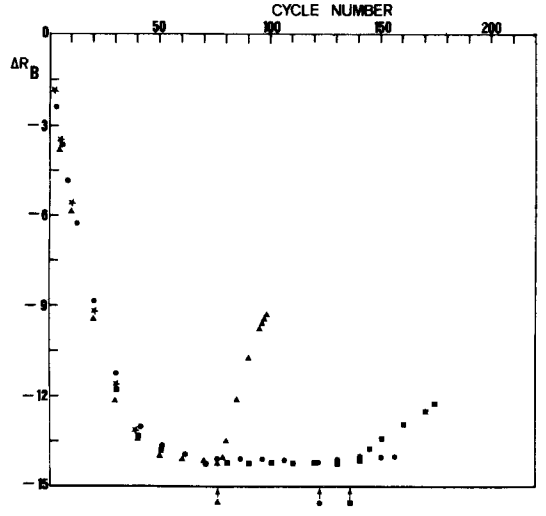

Fig. 12. Relative concentration variations at the bottom of the column with product withdrawal; reflux in mode I. $C_0 = 0.05$ mol dm^{-3}; $\Delta V/V_0 = 0.5$; $I = 0.6$ mA cm^{-2}. The symbols *, ▲, ■ and ● designate $\sigma/\Delta V$ equal to 0.00, 0.0625, 0.031 and 0.00625, respectively. The arrows mark the beginning of withdrawal in each case.

centration change is about five times smaller. This results undoubtedly from the fact that during the charging or discharging processes, the flowing solution does not have sufficient time to equilibrate with the electrodes before it is pumped through. This is unlike modes I and II where no overlap is allowed between the pumping and electrical steps. This mode is frequently applied in thermal parametric pumping [2].

In some experiments, limited product withdrawal was allowed after achieving steady state with total reflux. The results are depicted in Fig. 12 for various relative product outputs expressed by $\sigma/\Delta V$, where σ is the volume of the product sampled during a cycle. The profile reorganization towards a new lower output concentration is evident. It is clear that for relative product outputs smaller than 0.031, the column performance ceases to be affected by product withdrawal.

Finally, it is important to present the results of the mode I total reflux experiments (Figs. 6 and 7) in terms of the more dramatic concentration ratio C_B/C_T. This is done in Figs. 10 and 13. From the failure of symmetry shown in Fig. 6 it seems that the concentration ratio shown in Fig. 13 is depressed

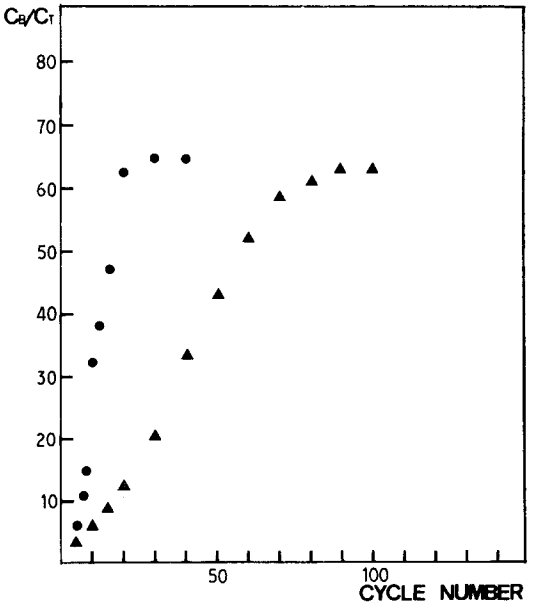

Fig. 13. Variation of the concentration ratio with the number of cycles; mode II experiments. $C_0 = 0.01$ mol dm^{-3}; $I = 0.6$ mA cm^{-2}; ●, $\Delta V/V_0 = 0.5$; ▲, $\Delta V/V_0 = 0.125$.

because of deactivation of those sections of the column held at low concentration. This presentation clearly shows that at low concentrations there is an inherent limit for the desalination power of the ECPP.

4. Concluding remarks

The dynamic properties of an electrochemical parametric pumping separation column were studied experimentally and theoretically, using the desalination of water as a test model. The combination of the parametric pumping concept with the electro-adsorptive properties of high surface carbon electrodes led to a new and powerful separation process. A remarkable feature of this combination is the utilization of a solid–liquid separation column in a continuous process.

Acknowledgement

We are thankful to Professor O. Kedem from the Weizmann Institute of Science and to Professor A. Apelblat from the Ben Gurion University, Beer Sheva, for helpful discussion.

Appendix

The solution of Equation 23 via Laplace transform.
The following expressions are used,

$$q^2 = rs; \quad r = 4Pl; \quad F(l) = f(l) - C_T \tag{A1}$$

where s is the Laplace parameter. The Laplace transform of Equation 23 is:

$$\frac{d^2\bar{V}}{dl^2} = q^2\bar{V} - rF(l)\,e^{-2Pl}, \tag{A2}$$

and the boundary conditions Equations 25 and 26:

$$\frac{d\bar{V}}{dl} = 2P\bar{V} \quad \text{for} \quad l = 0 \tag{A3}$$

and

$$\frac{d\bar{V}}{dl} = -2P\bar{V} \quad \text{for} \quad l = 1 \tag{A4}$$

where $\bar{V}$ is the transformed function of V. The general solution of Equation A2 is:

$$\bar{V} = A_1 e^{ql} + A_2 e^{-ql} - I_1 + I_2 \tag{A5}$$

where

$$I_1 = \frac{r}{2q} e^{ql} \int F(l)\, e^{-(2P+q)l} dl \tag{A6}$$

and

$$I_2 = \frac{r}{2q} e^{-ql} \int F(l)\, e^{-(2P-q)l} dl \tag{A7}$$

The constants A_1 and A_2 which were calculated from the boundary conditions, Equations A3 and A4, are:

$$A_1 = \frac{e^{-2q}H[-H(I_1)_0 + (I_2)_0] + [-(I_2)_1 H + (I_1)_1]\, e^{-q}}{1 - H^2 e^{-2q}} \tag{A8}$$

and

$$A_2 = \frac{[-H(I_1)_0 + (I_2)_0] + H e^{-q}[-(I_2)_1 H + (I_1)_1]}{H^2 e^{-2q} - 1} \tag{A9}$$

In the last two expressions:

$$H \equiv \frac{2P-q}{2P+q},$$

and $(I_1)_0$, $(I_1)_1$, $(I_2)_0$, $(I_2)_1$ are the corresponding boundary values of I_1 and I_2.

The inverse transform of Equation A5 leads back to the solution given in [16]. As a first approximation, $H^2\,e^{-2q}$ in the denominator of Equations A8 and A9 can be neglected relative to unity for high P and low T ($s \to \infty$ at $T \to 0$, cf. Equation A1).

An explicit expression for the initial condition $F(l)$ is necessary in order to obtain the inverse Laplace transform of Equation A5. We assume as a second approximation:

$$F(l) = B_0 + B_1 l. \tag{A10}$$

An approximation for any higher polynomial, say, for the third order, which was found adequate for S-shaped smooth functions [17], would immensely expand the treatment of Laplace transforms. The linear approximation (Equation A10) allows a derivation of the concentration gradient during one pumping step in a cycle from linear initial conditions only. It will be shown later that this is not a bad approximation as long as the adsorption curves (isotherms, isopotentiograms, etc.) show that the derivative $(\partial C_s/\partial \Delta E)_{C_f}$ is constant.

The final solution of the concentration profile after a backwards pumping step is obtained as follows: Equation A10 is substituted in Equations A6 and A7 which are then integrated to obtain:

$$I_1 = -(B_0 + B_1 l)\frac{re^{-2P}}{2q(2P+q)} - B_1\frac{re^{-2P}}{2q(2P+q)^2} \tag{A11}$$

and

$$I_2 = -(B_0 + B_1 l)\frac{re^{-2P}}{2q(2P-q)} - B_1\frac{re^{-2P}}{2q(2P-q)^2} \tag{A12}$$

Equations A8, A9, A11 and A12 are substituted in Equation A5 and the inverse Laplace transform of the resulting $V(l, T)$ expression is obtained. This is transformed (by means of Equation 22) back to the concentration profile $C_f(l, T)$, which was found to include tens of terms [18] and therefore will not be presented here.

References

[1] R. H. Wilhelm, A. W. Rice and A. R. Bendelius, *Ind. Eng. Chem.* 5 (1966) 141.
[2] P. C. Wankat, *Sep. Sci.* 9 (1974) 85.
[3] J. E. Sabadell and N. H. Sweed, *ibid.* 5 (1979) 171.
[4] A. A. Camero and N. H. Sweed, *AICHE J.* 22 (1976) 369.
[5] R. C. Rice, *Sep. Purif. Methods* 5 (1976) 139.
[6] S. W. Skarstrom, *Ann. N.Y. Acad. Sci.* 72 (1959) 75.
[7] R. H. Wilhelm, A. W. Rice, D. W. Rolke and N. H. Sweed, *Ind. Eng. Chem.* 7 (1968) 337.
[8] D. W. Thompson and D. Bass, *Can. J. Chem. Eng.* 52 (1974) 345.
[9] Y. Oren and A. Soffer, *J. Electrochem. Soc.* 125 (1978) 869.
[10] *Idem, J. Appl. Electrochem.* 13 (1983) 473.
[11] H. Kramers and G. Alberda, *Chem. Eng. Sci.* 2 (1953) 173.
[12] R. Gupta and N. H. Sweed, *I. E. Fundam.* 12 (1973) 335.
[13] A. Klingenberg and F. Sjenitzer, *Chem. Eng. Sci.* 5 (1956) 258.
[14] H. Brenner, *ibid.* 17 (1962) 229.
[15] P. V. Danckwerts, *ibid.* 2 (1953) 1.
[16] H. S. Carslaw and J. C. Yeager, 'Conduction of Heat in Solids', Oxford University Press, Oxford (1959) p. 114.
[17] B. Carnahan, H. A. Luther and J. O. Wilkes, 'Applied Numerical Methods', John Wiley and Sons. Inc. Chichester, New York (1969).
[18] Y. Oren, Ph.D. Thesis, the Weizmann Institute of Science (1978).
[19] H. R. C. Pratt, 'Countercurrent Separation Processes', Elsevier, Amsterdam (1967).